

# “Fifty-cent rheometer” for yield stress measurements: From slump to spreading flow

N. Roussel<sup>a)</sup>

*Division Bétons et Composites Cimentaires, Laboratoire des Ponts et Chaussées,  
75015 Paris, France*

P. Coussot

*Laboratoire des Matériaux et des Structures du Génie Civil, Institut Navier,  
77420 Champs sur Marne, France*

(Received 11 November 2004; final revision received 13 January 2005)

## Synopsis

The slump test, originally used to determine the “workability” of fresh concrete, has since been used in many industrial fields (e.g., mining and food industries). It offers a quick and easy way to measure the yield stress of suspensions or pasty materials. The model used for estimating the yield stress from the measured conical slump was first written by Murata [Mater. Struct. **98**, 117–129 (1984)], corrected by Schowalter and Christensen [J. Rheol., **42**, 865–870 (1988)] and adapted for a cylindrical geometry by Pashias [J. Rheol. **40**, 1179–1189 (1996)]. However, a discrepancy between experimental and predicted slumps still appears in the case of conical slumps [Clayton *et al.*, Int. J. Miner. Process. **70**, 3–21 (2003)] and for high-yield stress materials. In the present paper, we extend the theoretical analysis of this simple practical test by including different flow regimes according to the ratio between the radius ( $R$ ) and the height ( $H$ ) of the slumped cone. We propose analytical solutions of the flow for two asymptotic regimes, namely  $H \gg R$  and  $H \ll R$ . We finally compare the predictions of these solutions in terms of yield stress and previous expressions to three-dimensional numerical simulations and experimental data on a large range of yield stresses. This makes it possible to clarify the field of validity of the different approaches and provide further practical tools for estimating the yield stress of coarse materials. © 2005 The Society of Rheology. [DOI: 10.1122/1.1879041]

## I. INTRODUCTION

Many materials in industry or nature behave as fluids with a yield stress, which is the minimum stress for irreversible deformation and flow to occur. While the yield stress ( $\tau_c$ ) can be considered as a unique material property it may, of course, be measured using conventional rheological tools. However, this is not easy for many civil engineering materials containing coarse particles, and several specific large-scale apparatuses have been developed: Couette rheometers [Coussot and Piau (1995); Geiker *et al.* (2002) (“BML”)], parallel plates rheometers [De Larrard and Hu (1996) (“BTRheom”)]. These tests nevertheless often remain expensive and time consuming when only the yield stress

---

<sup>a)</sup> Author to whom all correspondence should be addressed; electronic mail: nicolas.roussel@lpc.fr

is needed for the industrial application. *In situ*, simpler and cheaper tests are still preferred which cannot be readily interpreted in rheological terms, i.e., they do not provide an intrinsic physical parameter of the material, but these tests have proved through the years to be able to *class* different materials in terms of their ability to be cast. One interesting category of *in situ* tests includes the so-called “slump tests.”

Typically, in a slump test a mold of a given conical shape is filled with the tested fluid. The mold is lifted and the material flows. If inertia effects can be neglected (see Sec. II C) it is generally admitted that the flow stops when the shear stress in the tested sample becomes equal to or smaller than the yield stress [Schowalter and Christensen (1998)]. Consequently, the shape at stoppage in the yielding region is directly linked to the material yield stress. From a practical point of view two geometrical quantities may be measured: the “slump” and/or the “spread.” The slump ( $S$ ) is the difference between the height of the mold at the beginning of the test ( $H_0$ ) and after flow stoppage. The spread is the final diameter of the collapsed sample. In most applications of the ASTM (1996) Abrams cone technique, the initial height of which is 30 cm, the slump is measured if it is smaller than 25 cm, otherwise the spread is measured. In the case of cement pastes, the yield stress of which is low compared to that of concrete, a smaller cone is used, namely the ASTM (2004) minicone technique. In that case the slump is typically of the same order as the initial height and only the spread is measured.

Several attempts to relate slump to yield stress may be found in the literature. They generally assume that the conical sample can be divided into two parts: above a critical height the shear stress remains smaller than the yield stress and no flow occurs; below this critical height the shear stress induced by the pressure due to the weight of material situated above is larger than the yield stress. In the latter region each layer of material widens until the pressure reaches a critical value for which the shear stress is equal to the yield stress. Following such an approach, Murata (1984) wrote a relation between the final height of the cone and the yield stress that does not depend on the mold geometry. Subsequent works established analogous relationships either for conical [Schowalter and Christensen (1998)] or cylindrical molds [Pashias *et al.* (1996)] with similar assumptions. These results were successfully validated by Clayton *et al.* (2003) and Saak *et al.* (2004) in the case of cylindrical molds. However, in the case of some conical molds or in the case of high-yield stress values (i.e., low slumps) with cylindrical molds, a discrepancy between predicted and measured slumps was systematically observed.

For large slumps the above approach likely does not apply since there is in general apparently no undeformed region, and the spread seems to be a more relevant parameter for estimating the material yield stress [Coussot *et al.* (1996); Domone (1998)]. Coussot *et al.* (1996), extending a two-dimensional solution of Liu and Mei (1989), wrote a solution (see Sec. III A) for this spreading problem for a yield stress fluid. This approach is based on the assumption that the depth of the fluid layer is everywhere much smaller than the characteristic length of the solid–liquid interface. Remarkably here, in contrast with the above-mentioned results for the slump, the yield stress is a function of the spread *and* the material volume.

All this shows that there remains some discrepancy between the different solutions proposed and experimental results, a discrepancy that we intend to clarify in this paper. First, we show that two very different regimes may be identified and that the incipient or stoppage flow conditions should be described with a proper three-dimensional yielding criterion (Sec. II). Then, we present two analytical solutions suitable for asymptotic regimes, namely large height-to-diameter ratio or large diameter-to-height ratio (Sec. III). We also carried out (Sec. IV) numerical simulations of the slump test for two classical conical geometries, the ASTM (1996) Abrams cone and the ASTM (2004) minicone.

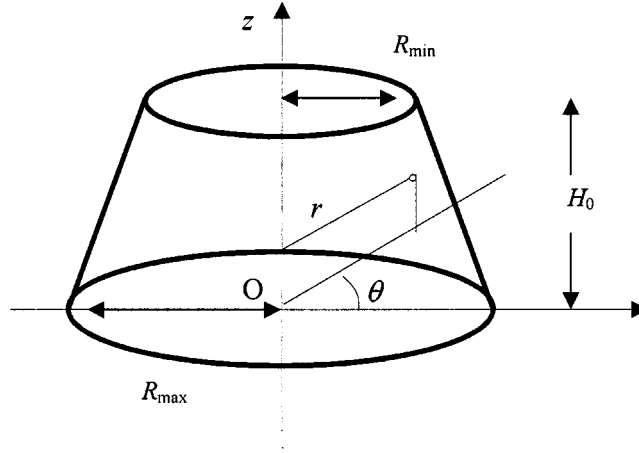


FIG. 1. Initial cone shape and cylindrical coordinates.

Finally, experimental results for the slump and the spread using the ASTM minicone with various material yield stresses are presented (Sec. V). We obtain an excellent agreement between the predicted and measured slumps over a wide range of dimensionless yield stresses, and we show that the analytical solutions well represent the reality in the two extreme cases of large or very small slumps.

## II. FLOW REGIME

### A. Generalities

Depending on flow characteristics two different parameters are measured (slump or spread) and very different theoretical approaches may be used (see above). This suggests that there exist two different flow regimes for which the stress tensor significantly differs. Let us examine that point in further detail. We describe the flow in the cylindrical coordinates attached to the horizontal solid surface  $(O, r, \theta, z)$  (see Fig. 1). The velocity components in the three corresponding directions are  $(v_r, v_\theta, v_z)$ . The symmetry of the problem implies that there is no tangential motion in a specific direction ( $v_\theta=0$ ) and that the variables do not depend on  $\theta$ . As a consequence, the strain rate tensor takes the general following form:

$$\mathbf{D} = \frac{\partial v_r}{\partial r} \mathbf{e}_{rr} + \frac{v_r}{r} \mathbf{e}_{\theta\theta} + \frac{\partial v_z}{\partial z} \mathbf{e}_{zz} + \frac{1}{2} \left( \frac{\partial v_r}{\partial z} + \frac{\partial v_z}{\partial r} \right) (\mathbf{e}_{rz} + \mathbf{e}_{zr}). \quad (1)$$

In the “slump” regime, since the sample height and diameter are of the same order of magnitude, the vertical and radial components of the velocity are of the same order. Consequently, none of the normal and tangential components of  $\mathbf{D}$  can *a priori* be neglected. On the contrary, in the “spread” regime, the flow thickness is much smaller than the radial extent of the sample, so we can expect the radial velocity to be much larger than the vertical velocity ( $v_z \ll v_r$ ) and that variations of flow characteristics in the vertical direction will be much more rapid than in the radial direction flow ( $\partial/\partial r \ll \partial/\partial z$ ). This corresponds to the long-wave (or lubrication) approximation, and in that case the strain rate tensor simplifies as

$$\mathbf{D} = \frac{1}{2} \frac{\partial v_r}{\partial z} (\mathbf{e}_{rz} + \mathbf{e}_{zr}). \quad (2)$$

Thus, the flow turns from a three-dimensional (with a cylindrical symmetry) to a one-dimensional flow as the fluid height becomes much smaller than its radial extent.

All previous analytical approaches (see the Introduction) used a one-dimensional expression of the constitutive equation including a one-dimensional yielding criterion

$$\dot{\gamma} = 0 \Leftrightarrow \tau < \tau_c, \quad (3)$$

in which  $\dot{\gamma}$  and  $\tau$  are the shear rate and shear stress magnitudes and  $\tau_c$  the fluid yield stress. Such an approach is nevertheless valid only when the flow is governed by the shear stress in some specific direction which, in our case, from (1), should occur only for large diameter-to-fluid thickness ratio. A similar problem is encountered with the squeeze flow of a cylindrical layer of material compressed between two disks. In that case the lubrication approximation was generally used [Covey and Stanmore (1981)] but led to the so-called “squeeze flow paradox”: due to the symmetry of the problem, the shear stress in the midplane equals zero so that the one-dimensional criterion (3) is fulfilled and the material should move as a rigid body (i.e., “plug flow”); however, Lipscomb and Denn (1984) have demonstrated that a plug region can only exist for uniform flows of yield stress fluids, which is obviously not the case for a squeeze flow since, due to mass conservation, the radial velocity increases with the distance from the central axis. Wilson (1993) pointed out that this paradoxical “yielded/unyielded” region is due to the neglect of the elongational stresses close to the midplane which are of an higher order than the shear stress. Consequently a proper three-dimensional criterion is thereafter needed to overcome this paradox and “a comprehensive yield criterion is one which is based upon a combination of all the acting components of the stress” [Adams *et al.* (1997)]. Generally, in this context, the Von Mises yielding criterion is used

$$\mathbf{D} = 0 \Leftrightarrow \sqrt{-T_{II}} < \tau_c, \quad (4)$$

in which  $T_{II}$  is the second invariant of the extra-stress tensor.

## B. Viscous and inertia effects

Here, we will assume that viscosity and inertia effects do not play any role in the slump at stoppage. This in particular means that the slump is not affected by the lift velocity of the mold, the flow inertia before stoppage, or the particular value of the “plastic” viscosity [or more generally the function  $F$  in Eq. (6)].

Although it is difficult to propose a general demonstration for that, it seems reasonable to assume that viscous effects do not play any role. Indeed, for sufficiently slow flows (in the absence of inertia effects) the yielding regions in the sample stop flowing when the yielding criterion (4) is exactly reached and the unyielding regions keep their initial shape, so that the final sample shape should basically depend on the yield stress value and the initial shape of the material.

Significant inertia effects may nevertheless induce an abrupt liquid–solid transition with yielding regions stopping flowing when the criterion (4) is not exactly reached. Let us compare the typical inertia stress ( $I = \rho V^2$ ) to the material yield stress. In the case of the ASTM Abrams cone, for a small slump, the flow duration is about 1 s for a slump of the order of 10 cm so that  $V \approx 0.1$  m/s. We thus have  $I \approx 20$  Pa, a value much smaller than the material yield stress in that case (typically larger than several hundred pascals). For a large slump the flow duration is about 5 s for a slump of the order of 20 cm, so that  $V$

$\approx 0.04$  m/s. We thus have  $I \approx 3$  Pa, a value much smaller than the material yield stress in that case (typically larger than several tens of pascals). These conclusions confirm the experimental deductions of Tatersall and Banfill (1983) and Murata (1984).

### C. Surface tension effects

Let us compare the viscous energy loss ( $dW_v$ ) to the surface energy change ( $dW_s$ ) during an elementary spreading (say, of  $dR$ ) over a solid surface of a horizontal layer of uniform thickness much smaller than its radial extent ( $H \ll R$ ). The surface energy change is the sum of the changes in the interfacial energy between the solid and the ambient gas ( $dW_{SG}$ ), the material and the ambient gas ( $dW_{LG}$ ), and the solid and the material ( $dW_{SL}$ ). These energies are proportional, respectively, to the changes in the surfaces of the solid–gas ( $dS_{SG}$ ), the material–gas ( $dS_{LG}$ ), and the solid–material ( $dS_{SL}$ ) interfaces, via a coefficient equal to the interfacial tension, respectively,  $\gamma_{SG}$ ,  $\gamma_{LG}$ ,  $\gamma_{SL}$ , which are related by the Young’s equation  $\gamma_{SG} = \gamma_{LG} \cos \theta + \gamma_{SL}$  [Young (1805)], where  $\theta$  is the wetting angle between the three phases. Since the thickness of the layer is small we have  $dS_{SG} \approx -dS_{LG} \approx -dS_{SL} \approx -2\pi R dR$ , from which we deduce that  $dW_s \approx 2\pi R \gamma_{LG} (1 - \cos \theta) dR$ . Note that from natural considerations  $\gamma_{LG}$  can be considered as typically equal to the surface tension of water with air, i.e., 0.07 Pa m. Assuming that the flow is mainly a simple shear flow in the radial direction, the shear strain ( $\gamma$ ) at a distance  $r$  is proportional to the shear strain at the periphery:  $r dR / RH$ , so that the total viscous energy loss is  $\int_{\Omega} \tau \gamma d\omega = \int_0^R \tau(r) dR / RH (2\pi H r dr)$ . In the limit of slow flows ( $\tau \approx \tau_c$ ) we find  $dW_v \approx 2\pi R^2 \tau_c dR / 3$ . Surface tension effects remain negligible when the energy loss due to viscous dissipation is much larger than the surface energy change, i.e., when  $dW_v \gg dW_s$ , which leads to the condition

$$\tau_c \gg \frac{3(1 - \cos \theta) \gamma_{LG}}{R}. \quad (5)$$

### III. ASYMPTOTIC FLOW REGIMES

Here, we develop the analytical solution of this flow problem in two asymptotic cases, namely  $H \gg R$  and  $R \ll H$ , in which  $H$  and  $R$  are the final height and radius of the sample. The constitutive equation beyond yielding is assumed to express in the general form [Oldroyd (1947)]

$$\Sigma = -p\mathbf{I} + \mathbf{T} = -p\mathbf{I} + \frac{\tau_c}{\sqrt{-D_{II}}} \mathbf{D} + F(\sqrt{-D_{II}}) \mathbf{D}, \quad (6)$$

in which  $D_{II}$  is the second invariant of the strain rate tensor and  $F$  a function which tends to zero when  $D_{II}$  tends to zero. In the following, the slump and the yield stress will be expressed in dimensionless form:

$$S' = \frac{S}{H_0}; \quad \tau'_c = \frac{\tau_c}{\rho g H_0}, \quad (7)$$

in which  $\rho$  is the material density,  $H_0$  the initial sample height, and  $g$  the gravity. It is worth noting that, although this scaling appeared quite suitable in the context of Pashias *et al.*'s (1996) and Schowalter and Christensen's (1998) approaches, a relationship between these variables independent of the initial sample geometry cannot be obtained in the general case. We will nevertheless use this scaling as it allows us to compare the results from theory or experiment with different geometries.

### A. Pure shear flow ( $H \ll R$ )

Here, we can describe the motion within the frame of the long-wave approximation. This situation was analyzed by Liu and Mei (1989) in the case of the two-dimensional slow flow of a viscoplastic fluid, then in the three-dimensional case by Coussot *et al.* (1996). The results were confirmed by the general approach of Balmforth *et al.* (2002). We look for the fluid depth at stoppage as a function of the distance:  $h(r)$ . When inertia effects can be neglected, Eqs. (2) and (6) show that, in the extra-stress tensor, only the tangential stress component  $\tau_{rz}$  is significant, so that the momentum equation simplifies as

$$0 = -\frac{\partial p}{\partial r} + \frac{\partial \tau_{rz}}{\partial z}; \quad 0 = -\rho g - \frac{\partial p}{\partial z}. \quad (8)$$

Integrating the second equation of (8) between 0 and  $z$  leads to the hydrostatic pressure distribution

$$p = \rho g(h(r) - z), \quad (9)$$

in which we took the atmospheric pressure as the reference pressure [ $p(h)=0$ ]. The first equation of (8) can then be integrated between 0 and  $h$ , which gives

$$\rho g h \frac{dh}{dr} = -\tau_{rz}(0). \quad (10)$$

At stoppage we have  $\tau_{rz}(0) \rightarrow \tau_c$ , so that (10) may be integrated taking into account the boundary condition  $h(R)=0$ . The cone shape at stoppage is not conical anymore but is described by

$$h(r) = \left( \frac{2\tau_c(R-r)}{\rho g} \right)^{1/2}. \quad (11)$$

It is worth noting that this shape is independent of the initial shape but depends on the sample volume. For example, from (11) we deduce  $H=h(0)=(2\tau_c R/\rho g)^{1/2}$ . Using (11) to compute the sample volume  $\Omega = \int_0^{2\pi} \int_0^R h(r) r dr d\theta$ , we also deduce an expression for the dimensionless yield stress as a function of the dimensionless slump

$$\tau'_c = \sqrt{\frac{2\pi}{15\Omega}} H_0^{3/2} (1-S')^{5/2}. \quad (12)$$

This result in particular confirms that the relationship between the dimensionless yield stress and slump also depends on geometrical characteristics of the sample.

We can also compute the expression for the spreading distance ( $R$ ) as a function of the yield stress and material volume

$$\tau_c = \frac{225\rho g\Omega^2}{128\pi^2 R^5}. \quad (13)$$

When the yield stress found from (13) is such that (5) is valid, we can conclude that surface tension effects are effectively negligible. This means that smaller yield stresses may be relevantly measured in this way by improving the wetting between the paste and the solid surface, i.e., by decreasing  $\theta$ . Ideally, with a perfect wetting ( $\theta=0$ ), infinitely small yield stresses might be measured.

**B. Pure elongational flow ( $R \ll H$ )**

Here, we consider a long cylinder of radius  $R$  much smaller than its length  $H$ . In that case the stress variations in the radial direction are negligible compared to those in the vertical direction. Let us consider the stress on a small layer of material at the height  $z$ . In the vertical direction it results from the weight of the material above and is equal to  $-\rho g(H-z)\mathbf{e}_z$ . The stress in the other direction (tangential and radial) is equal to zero. The local stress tensor is thus expressed as

$$\Sigma = -\rho g(H-z)\mathbf{e}_{zz} = -\frac{\rho g(H-z)}{3}\mathbf{I} + \frac{\rho g(H-z)}{3}(\mathbf{e}_{rr} + \mathbf{e}_{\theta\theta} - 2\mathbf{e}_{zz}). \quad (14)$$

The second term of the right-hand side is the extra-stress tensor. As long as the deformation remains small, the flow stops or starts for the critical height  $z_c$  at which the Von Mises criterion (4) is exactly reached which, taking into account (14), here leads to

$$\frac{\rho g(H-z_c)}{\sqrt{3}} = \tau_c. \quad (15)$$

Let us now assume that the overall shape of the sample is slightly affected by the corresponding flow in the yielded region. The final height ( $H=H_0-S$ ) is reached when no flow can occur even close to the solid surface, i.e.,  $z_c=0$ , and we obtain in dimensionless form

$$\tau'_c = \frac{(1-S')}{\sqrt{3}}. \quad (16)$$

In Fig. 5 we plotted this relation in a wide range of values of  $S'$  in order to have an idea of the trend it predicts, but one must keep in mind that Eq. (16) is *a priori* strictly valid only in the limit of small slump ( $S' \ll 1$ ). Note that a similar result would have been obtained by considering that the material undergoes a simple, uniaxial elongation.

**C. Intermediate case**

The above treatment of the pure elongational flow can be used to describe intermediate cases ( $R \approx H$ ), now within the frame of an approximate approach, which contrasts with the above rigorous treatments in the asymptotic cases. We consider that each horizontal layer of material locally undergoes, as a result of the weight of material above it, a simple elongation. We then assume that at each depth, after stoppage, the material layer has reached a radius  $R$  such that the Von Mises criterion is exactly reached. Now, one must take into account a reduced vertical stress  $\rho g(H_0-z)R_0^2/R(z)^2$ , in which  $R_0$  is the initial radius, and the final thickness ( $dZ$ ) of the layer is related to its initial thickness ( $dz$ ) via the mass conservation:  $R^2dZ=R_0^2dz$ . Following the final method of Pashias *et al.* (1996), one can then obtain by integration an explicit expression for the slump of a cylinder

$$S' = H' - \beta[1 + \ln(H'/\beta)], \quad (17)$$

in which  $\beta=\sqrt{3}$ . In fact, Pashias *et al.* (1996) obtained the same equation but with  $\beta=2$  because they assumed, in the context of their “one-dimensional” treatment of the problem, that yielding occurs when the maximum shear stress in the material (equal to half the vertical stress component) reaches the yield stress. This approach eventually appears to be equivalent to considering that the coefficient in (15) is 2 instead of  $\sqrt{3}$ . In the case of a cone an implicit equation providing the slump may be obtained [Schowalter

and Christensen (1998), Clayton *et al.* (2003)] again with a coefficient  $\beta$  which should be corrected in order to take into account the proper three-dimensional yielding criterion.

#### IV. NUMERICAL SIMULATIONS

Few authors developed numerical simulations of the slump test. Tanigawa and Mori (1989) carried out a visco-plastic finite-element analysis introducing a frictional interface law at the base of the slumping cone. They calculated the slump as a function of the yield stress but could not compare their results to experimental data. Schowalter and Christensen (1998) compared their own analytical prediction to the numerical results of Tanigawa and Mori and found a good agreement. Hu (1995), assuming that the shape of the deposit remains conical, calculated the stress distribution using an elastoplastic finite-element analysis. It must be emphasized that, although they considered the three-dimensional flow characteristics, all these approaches were based on a one-dimensional yielding criterion [of the type (3)].

Here, we used the computational fluid mechanics code FLOW-3D®, with which it is possible to implement a proper three-dimensional yield criterion. We describe the material behavior by an elasto-visco-plastic model: it behaves as an incompressible, simple, viscoelastic solid following the Kelvin–Voigt model up to the yield stress, beyond which it mainly behaves as a Bingham fluid, i.e., with a constitutive equation (6) in which  $F = 2\mu$ , where  $\mu$  is a constant. It is worth noting that, although it likely corresponds to the effective behavior of pasty materials, the viscoelastic solid regime does not play a fundamental role in the slump, and here it is basically a means to avoid the undetermination of the strain field in the unyielded regions. Other methods exist for the numerical simulations of yield stress fluid flows such as using a “biviscous” [Lipscomb and Denn (1984), O’Donovan and Tanner (1984)] or an exponential model [Papanastasiou (1987)] for the constitutive equation of the material, but the slump must be estimated from a regime transition (low to high viscosity), while in our approach the slump corresponds to the complete stoppage of the material.

Describing the rheological behavior either in elastic or viscous terms within a single fixed-grid model raises some problems: both the instantaneous velocity and the history of material points must be followed. Under these conditions FLOW-3D® contains logic within the scalar quantities that advects the properties of any quantity with the flow, via an incremental stress model. As the viscoelastic model is implemented explicitly, a stability criterion is also required to limit the time step necessary to achieve a numerically stable solution. Therefore, problems containing small cells and/or large values of the shear modulus have small time steps. In order to keep reasonable calculation time, we had to limit both the cell size and the elastic parameter.

From a numerical point of view, as already stated the value of the Young’s modulus of the material ( $E$ ) must be sufficiently small in order to limit the time of calculation, but it should also be sufficiently large for elastic deformations to remain negligible compared to viscous deformations. Finally, we found that a value of 1 MPa for the ASTM mini cone and a value of 10 MPa for the ASTM cone was a good compromise to fulfill the above two criteria. These values compare well with the experimental results of Saak *et al.* (2001) from dynamic tests, who measured for example 0.3 MPa for a water to cement powder weight ratio equal to 0.4.

The generated grid in the case of the ASTM minicone is shown in Fig. 2. A smaller cell size was used in the regions of largest deformations. The initial pressure distribution was assumed to be hydrostatic, and the speed at which the mold was “numerically” lifted was infinite since the mold simply disappeared at the initial time. In order to avoid any

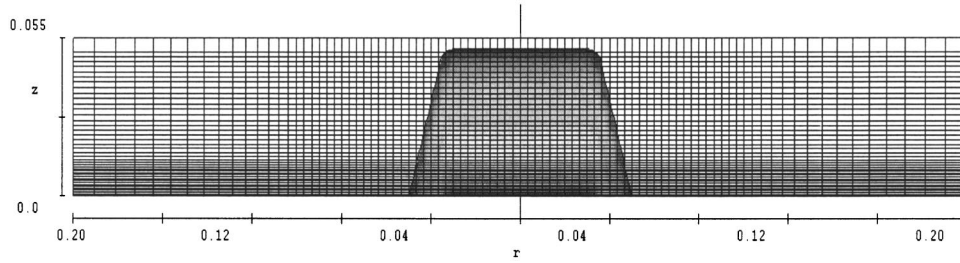


FIG. 2. Calculation grid for the numerical simulations in the case of the ASTM minicone.

non-negligible inertia effects that this calculus procedure might have induced, we used a relatively large plastic viscosity:  $\mu=300$  Pa s for the ASTM Abrams cone and  $\mu = 10$  Pa s for the ASTM minicone.

Typical predicted shapes in 3D for different yield stresses are shown in Fig. 3. The thickness vs radial distance for a large slump is shown in Fig. 4 and the numerical results in terms of dimensionless slumps vs dimensionless yield stress are plotted in Fig. 5.

**V. EXPERIMENTAL RESULTS**

Different materials were used (cement pastes or grouts and limestone powder suspension). The maximum particle size of these materials ( $100 \mu\text{m}$ ) was much smaller than the characteristic length of the mold and than the smallest final height after spreading (4 mm). The material yield stress was estimated independently, using a HAAKE ViscoTester® VT550 equipped with a vane geometry and following the procedure described by Nguyen and Boger (1985) with a rotation speed of  $0.4 \text{ rad min}^{-1}$ . Two different vane geometries were used, making it possible to measure the yield stress in a wide range (0.6 to 300 Pa) with an acceptable torque precision.

Slump measurements were carried out using the ASTM minicone geometry (see Table I). The plate surface was the same for all the tests. In order to prevent any thixotropic effect, the mold was lifted immediately after having been filled with the material. The mold was lifted relatively slowly in order to reduce possible inertia effects. The spread and slump measurements were done after 2 min. For each test, two perpendicular diameters and the maximum thickness of the collapsed sample were measured.

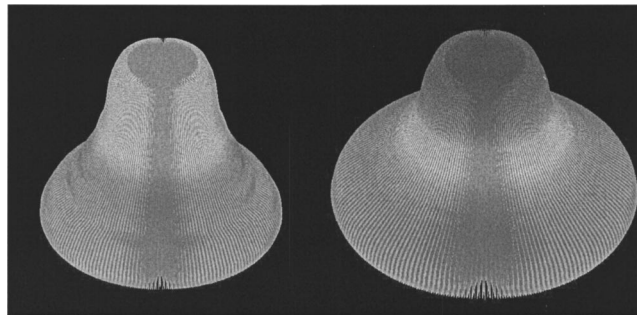
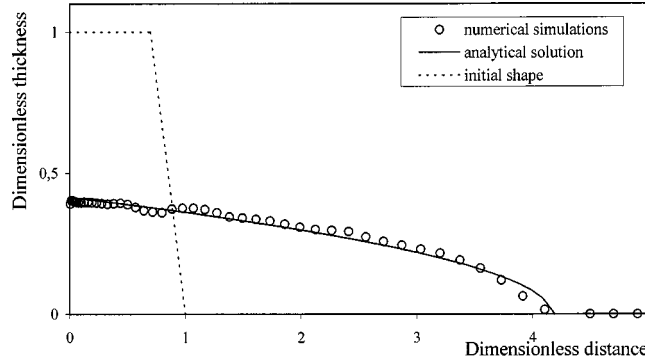


FIG. 3. Numerical simulations of slumped ASTM Abrams cones (final state) with two different yield stresses: 2600 Pa (left), 2000 Pa (right) (for a material density of  $2500 \text{ g/m}^3$ ).



**FIG. 4.** Final front shape as predicted by theory [Eq. (11)] and numerical simulations for a minicone test (the dotted line corresponds to the initial shape) and a material of dimensionless yield stress equal to 0.02: Dimensionless thickness (current thickness to initial height ratio) vs dimensionless distance (current distance to initial maximum radius ratio). Note the slight unexplained undulations of the free surface in the final numerical shape.

## VI. DISCUSSION

### A. Comparison between analytical, experimental, and numerical results

Our numerical results show that the slump effectively depends on the material yield stress and density, as expected from Schowalter and Christensen (1988), but also on the tested volume and the initial height since the numerical dimensionless slump differs for the two cone geometries [cf. Figs. 5(a) and 5(b)]. This confirms that the scaling suggested by Schowalter and Christensen (1998), although handy to plot results, is not appropriate for the general case. The comparison of the experimental spread with the analytical solution [Eq. (13)] for sufficiently large volumes (cf. Fig. 6) also shows the validity of the theoretical approach in the lubricational regime. Moreover, in that case the front shape as predicted by the theory [Eq. (11)] is in very good agreement with the numerical results (Fig. 4).

As expected, the “pure shear flow” solution [Eq. (12)] is close to numerical predictions for large slumps or low yield stresses, while the “pure elongational” solution [Eq. (16)] becomes valid for small slumps or large yield stress. More precisely, the pure elongational solution appears to be strictly valid only when the yield stress reaches the critical value for which flow does not occur ( $S' \rightarrow 0$ ) (see below). On the contrary, the pure shear flow solution remains an excellent approximation of the numerical results over a wide range of dimensionless yield stresses and slumps for both cone geometries, which confirms the relevance of the dependence on  $\Omega$  and  $H_0$  [Eq. (12)]. For both cone geometries studied here, it seems that this range is bounded by an upper value of the dimensionless yield stress value ( $\tau'_c = 0.03$  for the ASTM Abrams cone and  $\tau'_c = 0.02$  for the ASTM minicone) which corresponds roughly to  $H/R = 0.2$  for the two cones. However, it is worth noting that there remains some intermediate range in which none of the (asymptotic) analytical solutions is valid.

The agreement between numerical simulations and experimental results is very good [cf. Fig. 5(b)], which tends to prove that this code and the constitutive equation chosen for representing the material behavior are appropriate. This provides us with a useful tool to predict the result in the intermediate range for which none of the analytical solution appears suitable. It also appears (cf. Fig. 5) that the solution of Clayton *et al.* (2003) for the cone is not able to represent the data and the numerical predictions (as already stated by these authors).

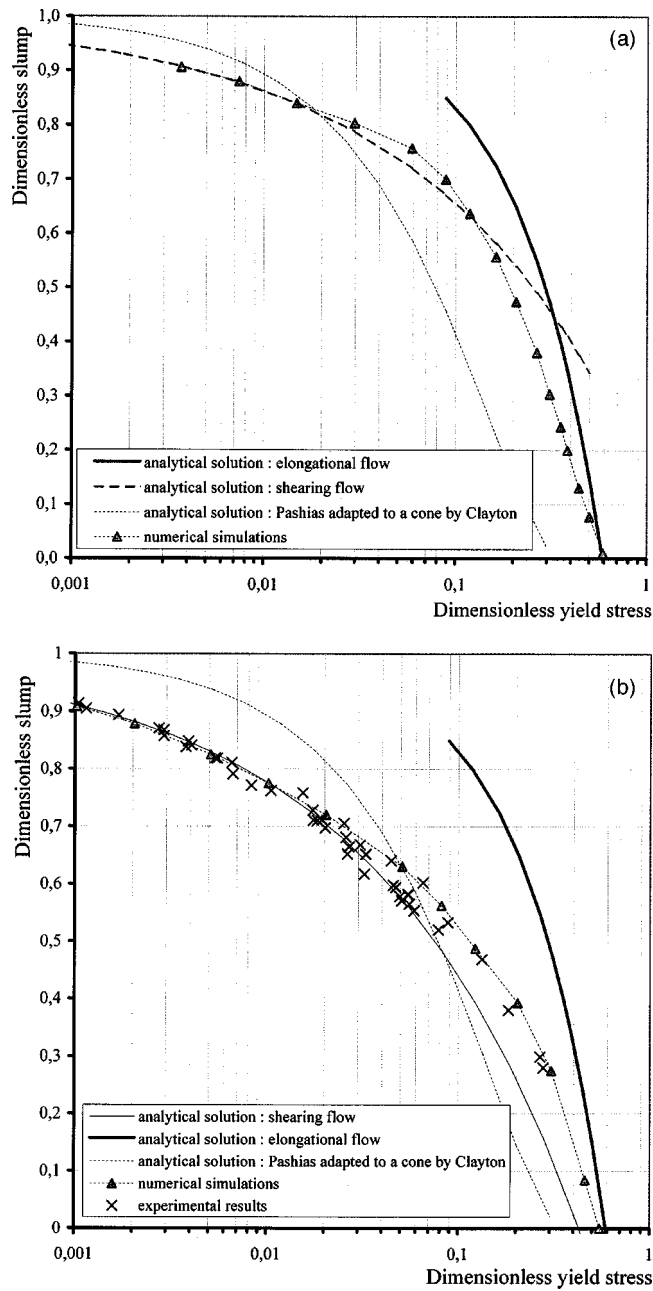


FIG. 5. Dimensionless slump in terms of dimensionless yield stress as predicted from numerical simulations, analytical approaches or obtained from experimental data (see the details in the text): (a) ASTM Abrams cone; (b) ASTM minicone.

**B. Critical yield stress**

The theoretical approach developed by Pashias *et al.* (1996) predicts a dimensionless critical yield stress equal to 0.5, but a discrepancy between experimental and analytical values was also observed by these authors. From a theoretical point of view we have

**TABLE I.** Cone characteristics.

Cone	ASTM Abrams cone	ASTM minicone
$H_0$ (mm)	300	50
$R_{\min}$ (mm)	50	35
$R_{\max}$ (mm)	100	50

shown [Eq. (16)] that for a pure elongational flow we should get a value of  $1/\sqrt{3} = 0.58$ . Such a result is valid either for a cylinder or a cone as long the sample height to radius ratio (aspect ratio) is sufficiently large. From our experiments with a conical sample with a moderate aspect ratio we also get a critical dimensionless yield stress around  $1/\sqrt{3}$ , but it is difficult to precisely determine this value which corresponds to an absence of flow because the material is always at least slightly deformed during mold lifting. At last, the value obtained from our numerical simulations, again with a moderate aspect ratio, is also surprisingly close to this value: 0.54 for the minicone and 0.59 for the Abrams cone. Recently, Chamberlain and co-workers (2003) measured the load needed to initiate a squeeze flow of an initially cylindrical sample. They computed the equivalent height of incipient failure, which is the height of material required for incipient flow, for a large range of cylinder radii. This is equivalent to calculating the critical yield stress for which flow starts or does not occur for a given cylindrical geometry. They studied the dependency of the critical yield stress on the cylinder radius. In the range of the ASTM minicone ( $R_{\max}/H_0=1$ ) and of the ASTM Abrams cone ( $R_{\max}/H_0=1/3$ ), they obtained dimensionless heights of incipient failure in the range  $[1.5;2]$ , which means that the dimensionless critical yield stress is in the range  $[0.5;0.66]$ . Although this result was obtained with a cylindrical shape and with a relatively small height to radius ratio, it is interesting to note that our theoretical, experimental, and numerical results fall in this range. To sum up, even for moderate aspect ratio the critical dimensionless yield stress is certainly higher than 0.50 as shown by the numerical and experimental results, and is not far from the theoretical value predicted from the pure elongational solution  $1/\sqrt{3}$ .

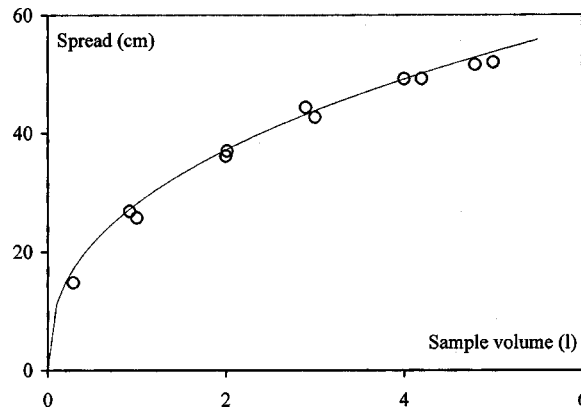


**FIG. 6.** Spread (here, the sample radius) as predicted by Eq. (13) (continuous line) and as obtained from various experimental tests (circles) in the case of a minicone and a sample of yield stress equal to 60 Pa.

### C. Sliding at the interface

The above analysis was carried out assuming no slip along the solid surface. The pure elongational solution does not depend on the boundary condition at the fluid bottom, but wall slip may affect the flow when one approaches the pure shear regime. In the experiments of Pashias *et al.* (1996) carried out with small particles, the influence of the conditions along the solid–liquid interface appeared negligible. In the case of concrete containing coarse particles, Tanigawa and Mori (1989) introduced in their numerical simulations a friction law at the liquid/solid interface but the influence of this additional parameter on the slump is not clear in their work. More recently, Chamberlain and co-workers (2003) studied the influence of the plate roughness on the critical yield stress assuming a Coulomb-type friction law at the interface involving a friction coefficient  $\mu_f$  equal to zero for a perfect slip case. They rigorously computed the stress field in a purely plastic cylindrical sample using either the Von Mises or Tresca plasticity criterion. They showed that, above a critical value  $\mu_c$  depending on the cylinder radius, there was no influence of the friction parameter on the height of incipient failure (or critical yield stress), and that the interface could then be considered as perfectly rough. They also showed that the difference between height of incipient failure predicted for the perfect slip ( $\mu_f=0$ ) and perfectly rough ( $\mu_c=0$ ) cases increased from zero for small radii to 18% for a radius equal to  $2\tau_0/\rho g$ . In the case of typical concrete, this reference radius becomes 0.16 m (yield stress around 2000 Pa and density around 2500 kg/m<sup>3</sup>). The radius of the ASTM Abrams cone being equal to 0.1 m, the error made by neglecting slip or friction at the interface in the case of concrete should be lower than 18% for low slumps.

## VII. CONCLUSION

We revisited the ability of existing analytical expressions for interpreting the slump test in rheological terms in the light of numerical simulations, theoretical considerations, and experimental results. Numerical simulations make it possible to predict experimental results very well and help us clarify the range of validity of these analytical expressions. For large slumps it is shown that only a pure shear flow approach is relevant. In particular, we showed that a three-dimensional yielding criterion should be taken into account to describe the pure elongational regime. Note that thixotropic effects were not taken into account in this study, but they may significantly affect data [Baudez *et al.* (2002)].

Finally, the slump test still appears a very good practical means for determining the yield stress of a material, but in the general case only a numerical approach could provide the yield stress by comparison with experimental data. In practice, the simplest and most appropriate means are experimental conditions making it possible to obtain either a large or a small slump depending on the material so as to use, respectively, Eq. (12) or (16) for determining the yield stress. Last, it is worth noting that these results apply for a yield stress material which can be considered as a continuum. When the presence of some granular phase makes it significantly deviate from a continuum, a rheological analysis of the slump or spread test in terms of a single, intrinsic, constitutive equation is impossible. This is, for example, the case when the ratio of fluid thickness to coarse particle size is not sufficiently large and/or when the concentration of grains is sufficiently large.

## References

- Adams, M. J., I. Aydin, B. J. Briscoe, and S. K. Sinha, “A finite element analysis of the squeeze flow of an elasto-viscoplastic paste material,” *J. Non-Newtonian Fluid Mech.* **71**, 41–57 (1997).  
 ASTM Designation C-143-90, “Standard Test Method for Slump of Hydraulic Cement Concrete,” in *Annual Book of ASTM Standards, 04.01* (Am. Soc. Test. Mat., Easton, MD, 1996), pp. 85–87.

- ASTM Designation C230/C230M-03, "Standard Specification for Flow Table for Use in Tests of Hydraulic Cement," in *Annual Book of ASTM Standards, 04.01* (Am. Soc. Test. Mat., Easton, MD, 2004).
- Balmforth, N. J., R. V. Craster, and R. Sassi, "Shallow viscoplastic flow on an inclined plane," *J. Fluid Mech.* **470**, 1–29 (2002).
- Baudez, J. C., F. Chabot, and P. Coussot, "Rheological interpretation of the slump test," *Appl. Rheol.* **12**, 133–141 (2002).
- Chamberlain, J. A., S. Clayton, K. A. Landman, and J. E. Sader, "Experimental validation of incipient failure of yield stress materials under gravitational loading," *J. Rheol.* **47**, 1317–1330 (2003).
- Clayton, S., T. G. Grice, and D. V. Boger, "Analysis of the slump test for on-site yield stress measurement of mineral suspensions," *Int. J. Min. Process.* **70**, 3–21 (2003).
- Coussot, P., and J. M. Piau, "A large-scale field coaxial cylinder rheometer to study the rheology of natural coarse suspensions," *J. Rheol.* **39**, 105–124 (1995).
- Coussot, P., S. Proust, and C. Ancey, "Rheological interpretation of deposits of yield stress fluids," *J. Non-Newtonian Fluid Mech.* **66**, 55–70 (1996).
- Covey, G. H., and B. R. Stanmore, "Use of the parallel plate plastometer for the characterization of viscous fluids with a yield stress," *J. Non-Newtonian Fluid Mech.* **8**, 249–260 (1981).
- De Larrard, F., and C. Hu, "The rheology of fresh high-performance concrete," *Cem. Concr. Res.* **26**, 283–294 (1996).
- Domone, P., "The slump flow test for high-workability concrete," *Cem. Concr. Res.* **28**, 177–182 (1998).
- Geiker, M. R., M. Brandl, L. N. Thrane, D. H. Bager, and O. Wallevik, "The effect of measuring procedure on the apparent rheological properties of self compacting concrete," *Cem. Concr. Res.* **32**, 1791–1795 (2002).
- Hu, C., "Rheology of fluid concrete," Ph.D. thesis, ENPC, Marne la Vallée, France, 1995 (in French).
- Lipscomb, G. G., and M. M. Denn, "Flow of Bingham fluids in complex geometries," *J. Non-Newtonian Fluid Mech.* **14**, 337–346 (1984).
- Liu, F. K., and C. C. Mei, "Slow spreading of a Bingham fluid on an inclined plane," *J. Fluid Mech.* **207**, 505–529 (1989).
- Murata, J., "Flow and deformation of fresh concrete," *Mater. Constr. (Paris)* **17**, 117–129 (1984).
- Nguyen, Q. D., and D. V. Boger, "Direct yield stress measurement with the vane method," *J. Rheol.* **29**, 335–347 (1985).
- O' Donovan, E. J., and R. I. Tanner, "Numerical study of the Bingham squeeze film problem," *J. Non-Newtonian Fluid Mech.* **15**, 75–83 (1984).
- Oldroyd, J. G., "A rational formulation of the equations of plastic flow for a Bingham solid," *Proc. Cambridge Philos. Soc.* **43**, 100–105 (1947).
- Papanastasiou, T. C., "Flows of materials with yield," *J. Rheol.* **31**, 385–404 (1987).
- Pashias, N., D. V. Boger, J. Summers, and D. J. Glenister, "A fifty-cent rheometer for yield stress measurements," *J. Rheol.* **40**, 1179–1189 (1996).
- Saak, A. W., H. M. Jennings, and S. P. Shah, "The influence of wall slip on yield stress and viscoelastic measurements of cement paste," *Cem. Concr. Res.* **31**, 205–212 (2001).
- Saak, A. W., H. M. Jennings, and S. P. Shah, "A generalized approach for the determination of yield stress by slump and slump flow," *Cem. Concr. Res.* **34**, 363–371 (2004).
- Schowalter, W. R., and G. Christensen, "Toward a rationalization of the slump test for fresh concrete: Comparisons of calculations and experiments," *J. Rheol.* **42**, 865–870 (1998).
- Tanigawa, Y., and H. Mori, "Analytical study on deformation of fresh concrete," *J. Eng. Mech.* **115**, 493–508 (1989).
- Tattersall, G. H., and P. G. F. Banfill, *The Rheology of Fresh Concrete* (Pitman, London, 1983).
- Wilson, S. D. R., "Squeezing flow of a Bingham material," *J. Non-Newtonian Fluid Mech.* **8**, 211–219 (1993).
- Young, T., "An essay on the cohesion of fluids," *Philos. Trans. R. Soc. London* **95**, 65–87 (1805).